

Quasi-Unidimensional $\{[M(\text{dmb})_2]Y\}_n$ Organometallic Polymers (M = Cu(I), Ag(I); dmb = 1,8-Diisocyano-*p*-menthane; Y = BF_4^- , PF_6^- , NO_3^- , ClO_4^- , CH_3CO_2^-).^{1a} Structural, Calorimetric, and Luminescence Properties

Daniel Fortin, Marc Drouin,^{1b} Martin Turcotte,^{1c} and Pierre D. Harvey*

Contribution from the Département de chimie, Université de Sherbrooke, Sherbrooke, Québec J1K 2R1, Canada

Received January 11, 1996. Revised Manuscript Received August 9, 1996[⊗]

Abstract: A series of new organometallic polymers of the type $\{[M(\text{dmb})_2]Y\}_n$ (dmb = 1,8-diisocyano-*p*-menthane; Y = BF_4^- , NO_3^- , ClO_4^- , M = Cu; Y = BF_4^- , PF_6^- , NO_3^- , CH_3CO_2^- , ClO_4^- ; M = Ag) are reported. These materials have been characterized from single-crystal X-ray diffraction (for $\{[\text{Ag}(\text{dmb})_2]Y\}_n$; Y = BF_4^- , NO_3^- , ClO_4^-), X-ray powder diffraction (which established the isostructurality between M = Cu and Ag and the relative crystallinity level), differential scanning calorimetry (DSC), solid-state magic spinning angle and solution ¹³C-NMR, and spin–lattice relaxation time measurements (T_1 , ¹³C-NMR). Three synthesis methods were employed in order to obtain highly crystalline, semicrystalline, and highly amorphous $\{[\text{Cu}(\text{dmb})_2]\text{BF}_4\}_n$ polymers. One polymer has been successfully characterized from a light-scattering technique. For the amorphous $\{[\text{Cu}(\text{dmb})_2]\text{BF}_4\}_n$ polymer, the molecular weights averaged 160 000. The Ag polymers are found to be rather crystalline and exhibit very low solubility properties. Except for the $\{[\text{Ag}(\text{dmb})_2]\text{PF}_6\}_n$ and the highly crystalline $\{[\text{Cu}(\text{dmb})_2]\text{BF}_4\}_n$ materials, all polymers exhibit glass transitions in the 37–96 °C (305–340 K) range, even if the materials exhibit a very large crystallinity level. The $\{[M(\text{dmb})_2]Y\}_n$ organometallic materials (M = Cu, Ag; Y = BF_4^- , PF_6^- , NO_3^- , CH_3CO_2^-) are also strongly luminescent in the visible range (400–600 nm) at 77 K, exhibiting polyexponential emission decay traces (either in the solid state or in solutions). By comparison with the emission properties of the non-polymeric $[\text{M}(\text{CN}-t\text{-Bu})_4](\text{BF}_4)$ compounds (M = Cu, Ag) as a model for a monomeric unit, the first and short-lived component of the emission decay traces (30–90% in relative intensity) is associated with a higher-energy emission localized at one M center within the polymer (“monomer-like emission”). This is also confirmed by time-resolved emission spectroscopy from the comparison with the emission maxima. The other components in the polyexponential decays are associated with lower-energy emissions that are only present in the polymers. This phenomenon is associated with an energy transfer metal-to-metal delocalized along the M chain somewhat similar to the exciton phenomenon known in organic solids. The depolarization of the emission light confirms the phenomenon. From density functional theory calculations, the lowest energy excited states have been assigned as MLCT (metal-to-ligand charge transfer) with the HOMO being the M centered d orbitals, and the LUMO being the π^* MO centered on the isocyanide groups. X-ray data for $\{[\text{Ag}(\text{dmb})_2]\text{BF}_4\}_n$: space group $P2_12_12_1$, orthorhombic, $a = 9.3273(18)$ Å, $b = 13.685(2)$ Å, $c = 22.124(4)$ Å, $V = 2824.0(9)$ Å³, $Z = 4$, $D_{\text{calc}} = 1.353$ g/cm³, $R = 0.068$, $R_w = 0.073$. $\{[\text{Ag}(\text{dmb})_2]\text{NO}_3 \cdot 0.70\text{H}_2\text{O}\}_n$: space group $P2_1/c$, monoclinic, $a = 13.1746(14)$ Å, $b = 9.7475(11)$ Å, $c = 23.207(3)$ Å, $\beta = 105.15(1)^\circ$, $V = 2876.5(6)$ Å³, $Z = 4$, $D_{\text{calc}} = 1.297$ g/cm³, $R = 0.051$, $R_w = 0.048$. $\{[\text{Ag}(\text{dmb})_2]\text{ClO}_4\}_n$: space group $P2_12_12_1$, orthorhombic, $a = 9.282(2)$ Å, $b = 13.772(2)$ Å, $c = 22.091(3)$ Å, $V = 2824.1(9)$ Å³, $Z = 4$, $D_{\text{calc}} = 1.282$ g/cm³, $R = 0.034$, $R_w = 0.077$.

Introduction

Over the past decade, research in the design of new materials has steadily increased, particularly in the area of ceramics,² liquid crystals,³ inorganic polymers,⁴ dendrimers,⁵ organic and inorganic conductors,⁶ new materials for nonlinear optical properties,⁷ and microelectronic devices.⁸ In a recent com-

munication the preparation of novel quasilinear organometallic polymers based upon the isocyanide chemistry, and using Ag as the multicoordinating center, was reported.^{1a} The synthesis of these new materials was achieved using the bidentate bridging dmb ligand (dmb = 1,8-diisocyano-*p*-menthane; Chart 1) which normally has a very strong tendency to form dimeric or trimeric compounds rather than polymeric species.⁹ These weakly

* To whom correspondence should be addressed.

[⊗] Abstract published in *Advance ACS Abstracts*, January 1, 1997.

(1) (a) A preliminary communication has already been reported: Perreault, D.; Drouin, M.; Michel, A.; Harvey, P. D. *Inorg. Chem.* **1992**, *31*, 3688. (b) Laboratoire de chimie structurale. (c) Undergraduate student.

(2) For examples see: *Chemistry of High-Temperature Superconductors*, Nelson, D. L., Whittingham, M. S., George, T. F., Eds.; ACS Symposium Series, No. 351; American Chemical Society: Washington, DC, 1987.

(3) Xu, B.; Swager, T. M. *J. Am. Chem. Soc.* **1993**, *115*, 1159.

(4) (a) Foucher, D. A.; Tang, B. Z.; Manners, I. *J. Am. Chem. Soc.* **1992**, *114*, 6246. (b) Liang, M.; Manners, I. *J. Am. Chem. Soc.* **1991**, *113*, 4044.

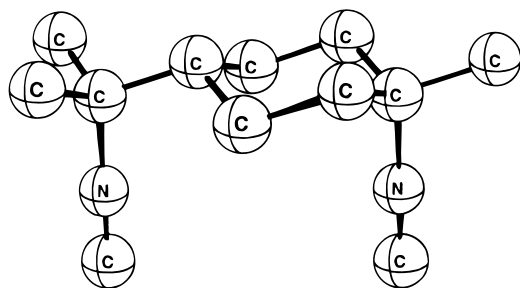
(5) (a) Wörner, C.; Mülhaupt, R. *Angew. Chem., Int. Ed. Engl.* **1993**, *32*, 1306. (b) Brabander-van den Berg, E. M. M.; Meijer, E. W. *Angew. Chem., Int. Ed. Engl.* **1993**, *32*, 1308.

(6) (a) *Organic and Inorganic Low-Dimensional Crystalline Materials*; Delhaes, P., Drillon, M., Eds.; Plenum Press: New York, 1987. (b) *Low-Dimensional Conductors and Superconductors*; Jérôme, D., Caron, L. G., Eds.; Plenum Press: New York, 1986.

(7) (a) Truong, K. D.; Grenier, P.; Houde, D.; Bandrauk, A. D. *Chem. Phys. Lett.* **1992**, *196*, 180. (b) Truong, K. D.; Bandrauk, A. D.; Tran-Thi, T. H.; Grenier, P.; Houde, D.; Palacin, S. *Thin Solid Films* **1994**, *244*, 981. (c) Pollagi, T. P.; Stoner, T. C.; Dallinger, R. F.; Gilbert, T. M.; Hopkins, M. D. *J. Am. Chem. Soc.* **1991**, *113*, 703. (d) Pollagi, T. P.; Geib, S. J.; Hopkins, M. D. *J. Am. Chem. Soc.* **1994**, *116*, 6051.

(8) See for example: Hickman, J. J.; Zou, C.; Ofer, D.; Harvey, P. D.; Wrighton, M. S.; Laibinis, P. E.; Bain, C. D.; Whitesides, G. M. *J. Am. Chem. Soc.* **1989**, *111*, 7271.

Chart 1



soluble materials exhibit needle-like or fibrous shapes, where the single-crystal X-ray structure reveals columnar parallel chains of $\text{Ag}(\text{dmb})_2$ units, isolated from each other by the counteranions (PF_6^- , BF_4^- , NO_3^- , ClO_4^-).^{1a} The 2,5-dimethyl-2',5'-diisocyanohexane ligand (tmb) is also known to form organometallic polymers with $\text{Ag}(\text{I})$.¹⁰ The polymers formed are three-dimensional materials, contrary to the dmb analogue. These materials were only characterized by X-ray diffraction techniques. During the search for new properties and applications for these polymeric compounds, this chemistry has been extended to the $\text{Cu}(\text{I})$ metal and two other counteranions (CH_3CO_2^- , ClO_4^-), notably with respect to the thermoplastic and luminescence properties. This study reports some structural features of several polymers (single crystal and powder diffraction), solid state properties (thermoplastic), along with a molecular weight determination (for one polymer), solid state ^{13}C -NMR analysis, and luminescence behavior. Relevant to the luminescence work, recently Chen and Archer¹¹ reported the synthesis and characterization of linear luminescent Schiff-base polyelectrolytes with $\text{Eu}(\text{III})$ in the backbone in which evidence for energy transfer is provided. The reported polymeric materials also exhibit energy migration along the backbone of the polymers.

Experimental Section

Material. The $\{[\text{Ag}(\text{dmb})_2]\text{Y}\}_n$ polymers ($\text{Y} = \text{PF}_6^-, \text{BF}_4^-, \text{NO}_3^-$) and the monomeric species $[\text{M}(\text{CN}-t\text{-Bu})_4]\text{BF}_4$ ($\text{M} = \text{Ag}, \text{Cu}$)¹² were prepared according to literature procedures except that acetonitrile was used. In the monomeric species, BF_4^- was used instead of ClO_4^- . The identity of the products was verified by chemical analysis. The nondeuterated solvents used (ethanol, Fisher, and acetonitrile, Aldrich) were purified according to procedures outlined in ref 13. The AgNO_3 , AgPF_6 , AgCH_3CO_2 , AgClO_4 , AgBF_4 , $\text{Cu}(\text{BF}_4)_2 \cdot \text{H}_2\text{O}$, $\text{Cu}(\text{ClO}_4)_2 \cdot 6\text{H}_2\text{O}$, and $\text{CN}-t\text{-Bu}$ were from Aldrich Chem. Co. These starting materials for synthesis were used as received.

(a) $\{[\text{Cu}(\text{dmb})_2]\text{BF}_4\}_n$. **Method 1.** In 50 mL of acetonitrile, 1.500 g (7.882 mmol) of dmb was dissolved in a 250-mL round flask. In a second round flask (100-mL), 0.670 g (2.63 mmol) of $\text{Cu}(\text{BF}_4)_2 \cdot \text{H}_2\text{O}$ was dissolved in 50 mL of acetonitrile. When the dilutions were completed, the second solution was added to the first and moderately stirred for 8 h. During this period the light blue color of the solution changed to a dark blue, then to orange, and then to a pale yellow-

brown, and did not change further. The resulting solution was concentrated down to 10–20 mL by evaporation, then was precipitated with diethyl ether. The beige deposit was filtered and redissolved in a minimum amount of acetone, and then reprecipitated with ether. The solid was again filtered and allowed to air dry. Yield ~99%. Chemical Anal. Theoretical: C, 53.28; H, 6.72; N, 10.04. Found: C, 53.84; H, 6.90; N, 9.92. $T_m = 165^\circ\text{C}$ dec. IR solid: 2169 cm^{-1} ($\text{C}\equiv\text{N}$). This method leads to high molecular weights and very amorphous polymeric materials.

Method 2. In a 250-mL round flask was dissolved 0.335 g (1.314 mmol) of $\text{Cu}(\text{BF}_4)_2 \cdot \text{H}_2\text{O}$ in 50 mL of acetonitrile. To it was added 1.000 g (1.574 mmol) of metallic copper under inert ($\text{N}_2(\text{g})$) atmosphere. The light blue solution slowly turned to light green (indicating the formation of $[\text{Cu}(\text{CH}_3\text{CN})_4]\text{BF}_4$) and was filtered (to remove the excess copper). A second solution was prepared in which 1.000 g (5.254 mmol) of dmb was dissolved in 50 mL of acetonitrile also under $\text{N}_2(\text{g})$ atmosphere. The second solution was added to the first one via a canular and stirred moderately for 8 h. The solution turned yellow-brown. After the reaction, the solution was concentrated down to 10–20 mL by evaporation. The beige solid was precipitated with diethyl ether and purified in the same way as stated above. Yield ~90%. Chemical Anal. Found: C, 53.70; H, 6.70; N, 9.67. This method leads to relatively low molecular weights and relatively more crystalline materials.

Method 3. This method is identical to method 2, except that the copper metal was not filtered after the reaction with dmb. Yield ~90%. The identity of the material was confirmed by comparing the spectroscopic data and chemical analysis to that of those prepared by methods 1 and 2. This method leads to highly crystalline materials with no glass transition.

(b) $\{[\text{Cu}(\text{dmb})_2]\text{ClO}_4\}_n$. In 50 mL of acetonitrile were dissolved 1.000 g (2.699 mmol) of $\text{Cu}(\text{ClO}_4)_2 \cdot 6\text{H}_2\text{O}$ and 1.540 g (8.10 mmol) of dmb in a 200-mL round flask. The light blue solution was stirred over 4 h, and a color change similar to that of $\{[\text{Cu}(\text{dmb})_2]\text{BF}_4\}_n$ prepared from method 1 occurred. After the reaction, the solution was filtered and concentrated down to 10–20 mL by evaporation. The beige solid was precipitated with diethyl ether and purified in the same way as stated above. Yield >90%. The polymer is light stable, but decomposes at $\sim 140^\circ\text{C}$. From X-ray powder diffraction analysis, this material is semicrystalline. IR solid: 2167 cm^{-1} ($\text{C}\equiv\text{N}$), 1087 cm^{-1} (ClO_4). $^1\text{H-NMR}$ (CD_3CN): δ 1.54 ppm (m).

(c) $\{[\text{Cu}(\text{dmb})_2]\text{NO}_3\}_n$. In 50 mL of methanol were dissolved 0.349 g (1.50 mmol) of $\text{Cu}(\text{NO}_3)_2 \cdot 2.5\text{H}_2\text{O}$ and 0.900 g (4.73 mmol) of dmb in a 200-mL round flask. The light blue solution was stirred over 4 h. The solution became clear and was concentrated down to ~ 10 mL by evaporation. The beige product was precipitated by addition of diethyl ether and purified in the same way as stated above. The solid was dried over 24 h under vacuum. Yield $\sim 100\%$. The polymer is light stable, but decomposes at $\sim 148\text{--}150^\circ\text{C}$. From X-ray powder diffraction analysis, this material is amorphous. IR solid: 2171 cm^{-1} ($\text{C}\equiv\text{N}$), 1361 cm^{-1} (NO_3). $^1\text{H-NMR}$ (CD_3CN): δ 1.54 (m). Chem. Anal. (Theoretical) C 56.95; H 7.17; N 13.84%. (Found) C 56.85; H 7.75; N 13.17%. The samples contain some water molecules as noticed in the IR and $^1\text{H-NMR}$ spectra, and from the X-ray results for $\{[\text{Ag}(\text{dmb})_2]\text{NO}_3 \cdot 0.70\text{H}_2\text{O}\}_n$ below.

(d) $\{[\text{Ag}(\text{dmb})_2]\text{CH}_3\text{CO}_2\}_n$. In 50 mL of acetonitrile, 1.500 g (7.882 mmol) of dmb was dissolved in a 200 mL round flask. In a second round flask (100 mL), 0.672 g (2.63 mmol) of “ $\text{Ag}(\text{CH}_3\text{CO}_2)$ ” was dissolved in 50 mL of acetonitrile. “ $\text{Ag}(\text{CH}_3\text{CO}_2)$ ” must be kept in the dark to avoid decomposition. Once the dilutions were completed, the second solution was added to the first and stirred moderately for 8 hours. After the reaction, the solution was filtered and concentrated down to 10–20 mL by evaporation. The white solid was precipitated with diethyl ether and purified in the same way as stated above. Yield $\sim 90\%$. Chemical Anal. Found: C, 56.6; N, 10.4; H, 7.3. Theoretical for $\text{C}_{26}\text{H}_{39}\text{N}_4\text{O}_2\text{Ag}$: C, 56.7; N, 10.2; H, 7.1. IR solid: 2187 cm^{-1} ($\text{C}\equiv\text{N}$). The polymer is light stable, but decomposes at $\sim 180^\circ\text{C}$. Crystalline materials can be obtained from slow vapor diffusion in acetone/ether for 10 h. The long needle-shaped crystals were too small for X-ray analysis.

(e) $\{[\text{Ag}(\text{dmb})_2]\text{ClO}_4\}_n$. This material was prepared according to the same procedure as for $\text{Y} = \text{PF}_6^-, \text{BF}_4^-, \text{NO}_3^-$.¹ Yield 90%. The

- (9) (a) Piché, D.; Harvey, P. D. *Can. J. Chem.* **1994**, *72*, 705. (b) Harvey, P. D.; Murtaza, Z. *Inorg. Chem.* **1993**, *32*, 4721. (c) Harvey, P. D.; Drouin, M.; Michel, A.; Perreault, D. *J. Chem. Soc., Dalton Trans.* **1993**, 1365. (d) Perreault, D.; Drouin, M.; Michel, A.; Harvey, P. D. *Inorg. Chem.* **1993**, *32*, 1903. (e) Che, C.-M.; Herstein, F. H.; Schaefer, W. P.; Marsh, R. E.; Gray, H. B. *Inorg. Chem.* **1984**, *23*, 2572. (f) Sykes, A. G.; Mann, K. R. *J. Am. Chem. Soc.* **1990**, *112*, 7247. (g) Boyd, D. C.; Matsch, P. A.; Mixa, M.; Mann, K. R. *Inorg. Chem.* **1986**, *19*, 3331.
- (10) Dartiguenave, M.; Dartiguenave, Y.; Mari, A.; Guitard, A.; Olivier, M. J.; Beauchamp, A. L. *Can. J. Chem.* **1988**, *66*, 2386.
- (11) Chen, H.; Archer, R. D. *Macromolecules* **1996**, *29*, 1957.
- (12) Bell, A.; Edwards, D. A. *J. Chem. Soc., Dalton Trans.* **1984**, 1317.
- (13) (a) Perrin, D. D.; Armarego, W. L. F.; Perrin, D. R. *Purifications of laboratory chemicals*; Pergamon: Oxford, U. K., 1966. (b) Gordon, A. J.; Ford, R. A. *The Chemist's Companion, a Handbook of Practical Data Techniques, and References*; Wiley: New York, 1972; p 436.

compound was characterized by single crystal crystallography. IR solid: 2130 and 2173 cm^{-1} ($\text{C}\equiv\text{N}$). Crystals suitable for X-ray analysis were obtained from slow diffusion of diethyl ether in acetonitrile solution.

(f) $\text{Cu}_2(\text{dmb})_2(\text{I})_2$. $\{[\text{Cu}(\text{dmb})_2]\text{BF}_4\}_n$ (1.000 g, 1.883 mmol of repetitive unit) was dissolved in 200 mL of acetonitrile, and to it was added 0.625 g (2.46 mmol) of I_2 . The mixture was stirred for 3 h. The solution was concentrated by evaporation to ~ 25 mL, then precipitated with diethyl ether. The yellow-beige solid was filtered and redissolved in a minimal amount of acetonitrile. The washing cycle was repeated until the residual ether became completely colorless (by IR no BF_4^- anion is detectable). Yield 70%. Crystals suitable for X-ray analysis were obtained from slow vapor diffusion of diethyl ether into a concentrated solution in ethanol. The identity of this product was confirmed from single crystal X-ray analysis as $\text{Cu}_2(\text{dmb})_2\text{I}_2 \cdot 2\text{CH}_3\text{CH}_2\text{OH}$ (Supporting Information). $T_m = 90^\circ\text{C}$.

(g) **Crystal Growth.** $\{[\text{Ag}(\text{dmb})_2]Y\}_n$ ($Y = \text{BF}_4^-, \text{NO}_3^-, \text{ClO}_4^-$). Crystals were obtained by vapor diffusion of diethyl ether into an acetonitrile solution of the polymer. $T_m^\circ(Y = \text{BF}_4^-) = 165\text{--}166^\circ\text{C}$ dec; $T_m^\circ(Y = \text{NO}_3^-) = 133\text{--}134^\circ\text{C}$ dec; $T_m^\circ(Y = \text{ClO}_4^-) = 168\text{--}170^\circ\text{C}$ dec. The crystals resembled long, narrow needles.

Instruments. The differential scanning calorimetry experiments were performed using a 5A DSC 7 Perkin Elmer instrument. The temperature was controlled using a $\text{N}_2(\text{l})$ bath and a 5B TAC 7/DS thermal analysis controller. The temperature calibration was done with indium and water samples. The precision was $\pm 0.1^\circ\text{C}$ for the temperature and $\pm 0.1\%$ for the calorimetric measurements. Typically each sample weighed from 5 to 10 mg and the scan rate was $10.0^\circ/\text{min}$. The DSC cells were two independent dual furnaces constructed of platinum–iridium alloy with independent platinum resistance heaters and temperature sensors. The X-ray powder diffraction patterns were measured using the Rigaku/USA instrument using a Cu irradiation tube operating at 40 KV and 30 MA. The UV–visible spectra were recorded on a Hewlett Packard 8452A diode array spectrometer. The luminescence spectra were obtained on either a steady-state LS-100 spectrofluorometer from Photon Technology Inc. or a Spex Fluorolog II spectrometer. Part of the emission lifetime measurements were also performed on the PTL LS-100 instrument. The second part was made using the Spex Fluorolog II spectrometer equipped with the Spex 1934 D phosphorimeter setup (for lifetimes that are at least 10 μs long). The chemical analysis measurements were performed at Guelph Chemical Laboratories Ltd. Both the decomposition phenomena and decomposition temperature have been confirmed using thermogravimetric analysis with a TGA7 Perkin Elmer Instrument. The measurements were performed within the 30–300 $^\circ\text{C}$ temperature range using a scan rate of 10 $^\circ\text{C}/\text{min}$, and were performed under Ar(g).

Molecular Weight Measurements. The average molecular weights in weight (M_w) were measured using light-scattering techniques. The dn/dc data (n = refraction index, c = concentration in g/10 mL) were acquired on an Optilab 903 differential refractometer from Wyatt Tech., and were measured at 298 K in acetonitrile or DMSO using concentrations going from 0.1% to 0.5% in weight. The average molecular weights in weight have been extracted from the Zimm plot obtained with a Wyatt Tech. DAWN F instrument at 298 K using acetonitrile or DMSO as solvents. The detectors (15 in total) covered the 26° to 129° angle range, and the laser was a He–Ne excimer laser (632.8 nm). The typical concentrations used for the measurements were between 0.07 and 0.30% in weight.

Spin–Lattice Relaxation Times (T_1). The T_1 's were measured by the inversion recovery pulse technique. The measurements were performed on a Bruker AC-F 300 NMR spectrometer operating at 75.47 MHz for carbon-13. The temperature was $\sim 21^\circ\text{C}$ and the sampling was done over a 20000 Hz sweep width using 8192 data points to describe the FID's. The solutions of the polymers were saturated in all cases in order to improve the signal-to-noise ratio. The uncertainties are $\sim 5\%$ on T_1 .

Computer Modelings. The molecular structure for 1,8-dicyano-*p*-menthane (instead of dmb) has been minimized using the commercially available PC MODEL MMX program (Serena Software).

X-ray Structural Studies. (a) $\{[\text{Ag}(\text{dmb})_2]\text{BF}_4\}_n$. Single-crystal X-ray data were collected at 200 K on an Enraf-Nonius CAD4 using graphite-monochromatized Cu $K\alpha$ radiation ($\lambda = 1.54178 \text{ \AA}$). The

cell parameters were determined using 24 reflections in the range of $60.0^\circ \leq 2\theta \leq 80.0^\circ$. Two standard reflections were measured after every 60 min to monitor instrument and crystal stability, but no significant decay was observed. Absorption corrections were applied based on ψ scan measurements on 9 azimuthal reflections. The NRCCAD¹⁴ programs were used for indexing data collection and cell measurements. The NRCVAX¹⁵ programs were used for data reduction, structure solution, and refinement. The scattering factors for all atoms and the anomalous-dispersion corrections were taken from the usual source.¹⁶ The structure was solved by the application of the direct methods and Fourier synthesis. The refinement was done by block-matrix least squares using anisotropic parameters for fully occupied atoms and isotropic thermal parameters for partially occupied atoms in the dmb ligand. Both of the independent ligands are disordered over two sets of sites.

A rigid body constraint was used for refinement including C2 to C12 (except C9) and C14 to C24 (except C21) atoms. In the first ligand the occupancies for the two orientations are 0.72/0.28; and for the second the occupancies are 0.57/0.43. Only major occupancy sites have been retained. The BF_4^- is also disordered and was treated as a B atom surrounded by two interlocking ideal tetrahedra of F atoms with B–F distances constrained to 1.336 Å , a 50:50 occupancy ratio was found. Only one site was retained. All H atoms were geometrically placed and not refined. The chirality was assigned¹⁷ according to Bijvoet differences and R_F values.

(b) $\{[\text{Ag}(\text{dmb})_2]\text{NO}_3\}_n$. A very fragile stick shaped crystal was chosen from several dried crystals trapped in an amorphous glass-like material. The amorphous material wrapped around the crystal was carefully removed. The single crystal data were collected at 169 K on an Enraf-Nonius CAD4 using graphite monochromatized Mo $K\alpha$ radiation ($\lambda = 0.70930 \text{ \AA}$). The cell parameters were determined using 24 reflections in the range of $30.0^\circ \leq 2\theta \leq 35.0^\circ$. Two standard reflections were measured every 60 min and 2% decay was observed. No correction was made for absorption. The NRCVAX programs were used for data reduction, structure solution, and refinement. The structure was solved by the application of the direct methods and successive Fourier difference synthesis.

Both independent ligands are disordered over two sets of sites. In the first ligand the occupancies of the two configurations are 0.737 and 0.263; in the second, the occupancies are 0.854 and 0.146. Only major occupancy sites were retained. The NO_3^- anion is also disordered over two sites. The occupancy refinement shows a 0.709/0.291 ratio. There is a partially occupied water molecule near the NO_3^- anion. Intermolecular distances suggest that only the NO_3^- anion with higher occupancy shares the cavity with the water molecule. The occupancy refinement of this water molecule converged to 0.70(2), which corresponds to the higher occupancy factor of the NO_3^- . Both of the NO_3^- anion sites were refined anisotropically using the GROUP option for coupled U parameter refinement included in the NRCVAX least-squares refinement program.

(c) $\{[\text{Ag}(\text{dmb})]\text{ClO}_4\}_n$. The structure was solved by the application of direct methods using the NRCVAX crystal structure determination system and refined using SHELXL-93. The dmb ligand is disordered over two sets of sites with an occupancy ratio of 0.531(7)/0.469(7), and only the dmb with higher occupancy factors have been retained. The ClO_4^- is also disordered in a 50:50 ratio, and only one site was retained.

The crystal data are available in Table 1.

Theoretical Calculations. The reported density functional calculations were all carried out using the program called AMOL which was developed by Baerends *et al.*^{18,19} and vectorized by Ravenek.²⁰ The numerical interaction procedure applied for the calculations was

(14) Le Page, Y.; White, P. S.; Gabe, E. J. NRCCAD, An enhanced CAD-4 control program. *Proc. Am. Crystallogr. Hamilton Meeting*, Abstract PA 23, 1986.

(15) Gabe, E. J.; Le Page, Y.; Charland, J.-P.; Lee, F. L.; White, P. S. J. *Appl. Crystallogr.* **1989**, *22*, 384.

(16) *International Tables for X-ray Crystallography*; Kynoch Press: Birmingham, England, 1974; Vol. IV.

(17) Rogers, D. *Acta Crystallogr.* **1981**, *A37*, 734.

(18) Baerends, E. J.; Ellis, D. E.; Ros, P. *Chem. Phys.* **1973**, *2*, 41.

(19) Baerends, R. J. Ph.D. Thesis, Vrije Universiteit, Amsterdam, 1975.

Table 1. Crystallographic Data

	$\{[\text{Ag}(\text{dmb})_2]\text{BF}_4\}_n$	$\{[\text{Ag}(\text{dmb})_2]\text{NO}_3 \cdot 0.70\text{H}_2\text{O}\}_n$	$\{[\text{Ag}(\text{dmb})_2]\text{ClO}_4\}_n$
formula	$\text{AgC}_{24}\text{H}_{36}\text{N}_4\text{BF}_4$	$\text{AgC}_{24}\text{H}_{36}\text{N}_5\text{O}_3 \cdot 0.70\text{H}_2\text{O}$	$\text{AgC}_{24}\text{H}_{36}\text{N}_4\text{ClO}_4$
F_w	575.25	507.12	587.89
F_{000}	1184	1174	1216
space group	$P2_12_12_1$	$P2_1/c$	$P2_12_12_1$
cryst syst	orthorhombic	monoclinic	orthorhombic
$a, \text{\AA}$	9.3273(18)	13.1746(14)	9.282(2)
$b, \text{\AA}$	13.685(2)	9.7475(11)	13.772(2)
$c, \text{\AA}$	22.124(4)	23.207(3)	22.091(3)
β, deg	90	105.152(9)	90
Z	4	4	4
T, K	193	168	193
$\lambda(\text{K}\alpha_{\text{ax}}), \text{\AA}$	1.54184	0.71073	0.71073
$D_{\text{cal}}, \text{g/cm}^3$	1.353	1.302	1.383
μ, cm^{-1}	62.08	7.24	8.4
transmission coeff	0.5822, 0.9991	0.9110, 0.9954	
$R(F_o)^a$	0.068	0.051	0.034
R_w^b	0.073	0.048	0.077 ^c

^a $R(F_o) = \sum(F_o - F_c)/\sum(F_o)$. ^b $R_w = [\sum(w(F_o - F_c)^2)/\sum(wF_o^2)]^{1/2}$. ^c $R = (F_o^2 + 2F_c^2)/3$.

developed by te Velde *et al.*²¹ The electronic configurations of the molecular systems were described by an uncontracted triple- ζ basis set²² on silver for 4d, 5s, and 5p. Double- ζ STO basis sets^{23,24} were used for carbons (2s, 2p), nitrogen (2s, 2p), and hydrogen (1s), augmented with a single 3d polarization function except for hydrogen where a 2p function was used. Polarization functions were not used for silver. The $1s^2 2s^2 2p^6 3s^2 3p^6$ configuration on silver, and the $1s^2$ configuration on carbon and nitrogen were assigned to the core and were treated by the frozen-core approximation.¹⁹ A set of auxiliary²⁵ s, p, d, f, and g STO functions, centered on all nuclei, was used in order to fit the molecular density and present the Coulomb and exchange potentials accurately in each SCF cycle. Energy differences were calculated by combining the local exchange-correlation potential by Vosko *et al.*²⁶

Polarization. The polarization ratios (N) were measured according to literature procedures.²⁷ The polarization ratio, N , is given by $(I_v/I_H)_v/(I_H/I_v)_H$. $(I_v/I_H)_v$ is the ratio of the intensities of vertically to horizontally polarized emissions when excited with vertically polarized light, and $(I_H/I_v)_H$ is the ratio of the intensities of horizontal and vertical emissions with horizontally polarized excitation. N is related to the relative orientation of transition moments in absorption and emission. The theoretical value of $N = 3$ indicates that the absorption is polarized along a single molecular axis followed by an emission along the same axis. $N = 0.5$ indicates single-axis absorption followed by emission along a perpendicular axis. (In practice, these theoretical values were never obtained; this is due in part to the natural depolarization of the glass.) In the special case where $N = 1$, the emission is considered to be depolarized.

(20) Ravenek, W. *Algorithms and Applications on Vector and Parallel Computers*; Rigie, H. J. J.; Dekkor, Th. J., van de Vorst, H. A., Eds.; Elsevier: Amsterdam, 1987.

(21) Boerrigter, P. M.; te Velde, G.; Baerends, E. J. *Int. J. Quantum Chem.* **1988**, *33*, 87.

(22) (a) Snijders, G. J.; Baerends, E. J.; Vernooys, P. *At. Nucl. Data Tables* **1982**, *26*, 483. (b) Bernooy, P.; Snijders, G. J.; Baerends, E. J. *Int. Slater Type Basis Functions for the Whole Periodic System*; International report; Free University of Amsterdam: Amsterdam, 1981.

(23) (a) Noodleman, L.; Norman, J. G. *J. Chem. Phys.* **1979**, *70*, 4903. (b) Noodleman, L. *J. Chem. Phys.* **1981**, *74*, 5737. (c) Noodleman, L.; Baerends, E. J. *J. Am. Chem. Soc.* **1984**, *106*, 2316.

(24) Noodleman, L.; Baerends, E. F. *J. Am. Chem. Soc.* **1984**, *106*, 2316.

(25) Krijn, J.; Baerends, E. J. In *Fit Function in the JFS-method*; Internal Report (in Dutch); Free University of Amsterdam: Amsterdam, 1984.

(26) Vosko, S. D.; Wilk, L.; Nusair, M. *Can. J. Phys.* **1990**, *58*, 1200.

(27) See for examples: (a) Zelent, B.; Harvey, P. D.; Durocher, G. *Can. J. Spectrosc.* **1984**, *29*, 23. (b) *Can. J. Spectrosc.* **1983**, *28*, 188. (c) Harvey, P. D.; Zelent, B.; Durocher, G. *Spectrosc. Int. J.* **1983**, *2*, 128 and references therein. (d) Brummer, J. G.; Crosby, G. A. *Chem. Phys. Lett.* **1984**, *112*, 15.

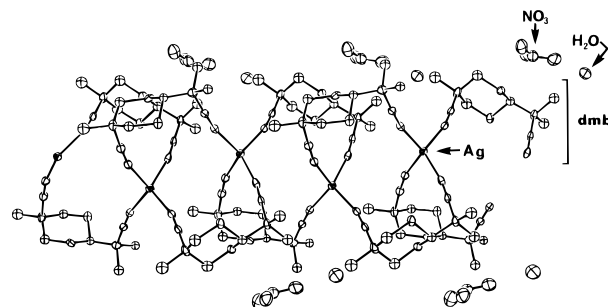
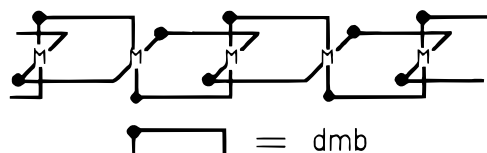


Figure 1. X-ray structure of the $\{[\text{Ag}(\text{dmb})_2]\text{NO}_3 \cdot 0.70\text{H}_2\text{O}\}_n$ polymer. Only a fraction of the chain is represented (~ 5 $[\text{Ag}(\text{dmb})_2]\text{NO}_3$ units). The ORTEP is shown at 50% probability and the hydrogen atoms are not shown for clarity.

Chart 2

Results and Discussion

1. X-ray Single Crystals. The $\{[\text{Ag}(\text{dmb})_2]\text{Y}\}_n$ materials ($\text{Y} = \text{BF}_4^-, \text{NO}_3^-, \text{ClO}_4^-$) exhibit a polymeric tubular structure in the solid state (Chart 2). The polymeric chains crystallize side by side separated by rows of BF_4^- , NO_3^- , or ClO_4^- counteranions (Figure 1; NO_3^- as an example). The silver atoms are tetraordinated in a distorted tetrahedral fashion. All metal atoms are bridged by dmb ligands, two bridging each neighboring metal. The silver atoms do not form a straightline chain. Instead they form a zigzag structure with an angle that varies only slightly with the nature of the counteranion: $\text{Y} = \text{PF}_6^-$, $\angle = 139.15(4)^\circ$;^{1a} $\text{Y} = \text{BF}_4^-$, $\angle = 140.46(2)^\circ$; $\text{Y} = \text{NO}_3^-$, $\angle = 139.88(1)^\circ$; $\text{Y} = \text{ClO}_4^-$, $\angle = 139.57(2)^\circ$. No close $\text{Ag}\cdots\text{Ag}$ contact is observed. The $\text{Ag}\cdots\text{Ag}$ separations are approximately 5 Å, a distance that is far from the sum of the van der Waals radii (3.40 Å).²⁸ Unlike the AgAgAg angle, the $\text{Ag}\cdots\text{Ag}$ separations vary somewhat more from one polymer to another: $\text{Y} = \text{PF}_6^-$, $d(\text{Ag}\cdots\text{Ag}) = 4.964(1)$ Å;^{1a} $\text{Y} = \text{BF}_4^-$, $d(\text{Ag}\cdots\text{Ag}) = 4.9557(9)$ Å; $\text{Y} = \text{NO}_3^-$, $d(\text{Ag}\cdots\text{Ag}) = 5.1884(6)$ Å; $\text{Y} = \text{ClO}_4^-$, $d(\text{Ag}\cdots\text{Ag}) = 4.9496(1)$ Å. This variation cannot be correlated with the temperature of the measurements. The $d(\text{Ag}\cdots\text{Ag})$ data for PF_6^- , BF_4^- , and ClO_4^- are very similar (~ 4.96 Å), while the NO_3^- value differs slightly (~ 5.19 Å). The only major difference is the presence of 0.70(2) water molecules per Ag unit in the NO_3^- polymer forming dimeric H-bonded $(\text{NO}_3\cdots\text{H}_2\text{O})_2$ species. The presence of H bonding (Figure 1, $d(\text{O}_2\text{NO}\cdots\text{OH}_2) = 2.804(23)$ and $2.814(16)$ Å) and a different space group could be the root of this difference.

The longest $\text{M}\cdots\text{M}$ separation ever reported for a dmb complex is 5.284(2) Å,²⁹ a compound in which Ag monocations are encapsulated inside $\text{Ir}_2(\text{dmb})_4^{2+}$ dimeric species. This value is ~ 0.096 Å, longer than that found in the $\{[\text{Ag}(\text{dmb})_2]\text{NO}_3 \cdot 0.70\text{H}_2\text{O}\}_n$ polymer. On the other hand, the shortest $\text{M}\cdots\text{M}$ distances reported (based upon X-ray results) are 2.986(2) Å for $[\text{Ir}_2(\text{dmb})_4(\text{PPh}_3)(\text{AuPPh}_3)]^{3+}$ ³⁰ and 2.72 ± 0.05 Å for M_2 -bonded d^9-d^9 $\text{Pd}_2(\text{dmb})_2\text{X}_2$ complexes ($\text{X} = \text{Cl}^-, \text{Br}^-$), based upon spectroscopic (Raman and UV-vis) measurements.^{9b} Recently, Miskowski, Gray, Mann, *et al.* reported MM2-type calculations on the $\text{Rh}_2(\text{dmb})_4^{2+}$ complex,

(28) Cotton, F. A.; Wilkinson, G.; Gaus, P. D. *Basic Inorganic Chemistry* 3rd ed.; Wiley: Toronto, 1995; p 61.

(29) Sykes, A. G.; Mann, K. R. *J. Am. Chem. Soc.* **1988**, *110*, 8252.

(30) Sykes, A. G.; Mann, K. R. *J. Am. Chem. Soc.* **1990**, *112*, 7247.

Chart 3

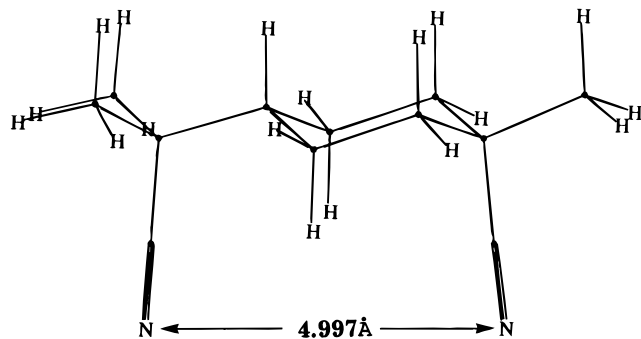
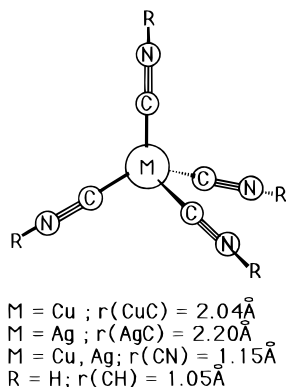


Chart 4



both in the ground and $^3A_{2g}$ excited states.³¹ The minimum energy surfaces were found to be very shallow exhibiting minima at 4.75 and 3.5 Å in the ground and excited states, respectively. Energy minimization of the 1,8-dicyano-*p*-menthane ligand (instead of dmb) was computed using the MMX program.³² The resulting N...N separation is 4.997 Å (Scheme III), a value that is very close to the M...M separation found in the polymers. This result suggests that the formation of the polymers does not induce any major uphill energy dmb configuration.

The average Ag-C (2.20 Å), C≡N (1.15 Å), and N-C (1.47 Å) bond distances are normal (see Supporting Information) as they compare favorably to that reported for the $\text{Ag}_2(\text{dmb})_2\text{X}_2$ complexes (X = Cl, Br, I), average $d(\text{Ag}-\text{C}) = 2.15$ Å and average $d(\text{C}\equiv\text{N}) = 1.13$ Å.^{9d}

2. X-ray Powder Diffraction. In order to establish the isostructural nature of the $\{[\text{Cu}(\text{dmb})_2](\text{BF}_4)_n\}$ polymer, the X-ray powder diffraction patterns have been investigated. The X-ray powder diffraction patterns for both polymers (M = Cu (method 2) and Ag) show a fairly good correspondence between the spectra, indicating their isostructurality. Only some minor differences are noticed concerning the relative intensity ratios. The analysis of these patterns is provided in the Supporting Information, where the 2θ , values (calculated and observed) are included along with the indexation data. The comparison between the unit cell parameters extracted from the single crystal X-ray structures and the X-ray powder diffraction patterns for a given polymer is excellent (Supporting Information), thus providing a fairly high degree of reliability on the M = Cu

(31) Miskowski, V. M.; Rice, S. F.; Gray, H. B.; Dallinger, R. F.; Milder, S. J.; Hill, M. G.; Exstrom, C. L.; Mann, K. R. *Inorg. Chem.* **1994**, *33*, 2799.

(32) The MMX program places a positive charge on the N atom of the C-N≡C group due to the tetravalent nature of the atom. As a result the program computes electrostatic interactions and the C...C separations (bite distances) > 5.2 Å. By replacing the isocyano groups by cyano or acetylene (-C≡C-H) the bite distance decreases to ~5 Å.

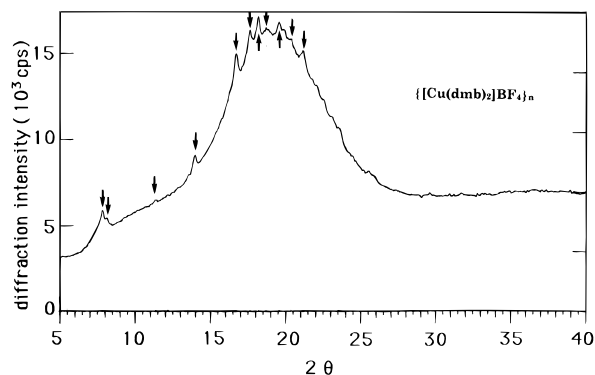


Figure 2. X-ray powder diffraction pattern for an amorphous sample of $\{[\text{Cu}(\text{dmb})_2]\text{BF}_4\}_n$ prepared from method 1. Completely structureless spectra have been obtained for other samples. This example has been chosen to show the small crystalline portion establishing the identity of the polymer.

data. The change in unit cell volume ($\{[\text{Ag}(\text{dmb})_2]\text{PF}_6\}_n$, 2924 Å³ > $\{[\text{Ag}(\text{dmb})_2]\text{BF}_4\}_n$, 2876 Å³ > $\{[\text{Cu}(\text{dmb})_2]\text{BF}_4\}_n$, 2826 Å³ (powder data)) is consistent with the volume difference between the counteranions and metals (i.e. $\text{PF}_6^- > \text{BF}_4^-$, Ag > Cu).

During the course of these studies, different samples of the $\{[\text{Cu}(\text{dmb})_2]\text{BF}_4\}_n$ polymer were prepared and analyzed (methods 1, 2, and 3). The samples prepared from method 1 were very amorphous giving X-ray powder diffraction patterns similar to that shown in Figure 2. There is no major change in molecular weight ($127\,000 < M_w < 192\,000$; section below) between the samples prepared from method 1. The only difference is presumably the M_w distribution that is detected from the variation in signal within the DSC curves discussed further below. The $\{[\text{Cu}(\text{dmb})_2]\text{BF}_4\}_n$ materials prepared according to method 3 exhibit the highest level of crystallinity similar to that of the $\{[\text{Ag}(\text{dmb})_2]\text{BF}_4\}_n$ polymer.^{33,34}

The crystallinity of the samples increases slowly with time over a period of several days, where increases of 5 to 50% in peak intensity (depending on the counteranions) are observed. Upon heating, the rate of crystallinity increment increases greatly, even above the T_g (described below).

3. Molecular Weight Determination. The molecular weights (M_w) for the $\{[\text{Cu}(\text{dmb})_2]\text{BF}_4\}_n$ polymer samples prepared from method 1 in acetonitrile at 298 K have been determined by light

(33) We have attempted to obtain fine tuning in the control of crystallinity of the polymers. First, the change in M/dmb stoichiometry (1:2, 1:2.1, 1:excess) did not change the crystallinity. The change in reaction temperature (from -20 to +45 °C) also did not influence the relative crystallinity. Finally, method 1 provides almost entirely amorphous $\{[\text{Cu}(\text{dmb})_2]\text{BF}_4\}_n$ materials. The relative ratio of the crystalline/amorphous portion can be slightly modified with the reaction times. At short times (ca. a few minutes) the material is highly amorphous, but the X-ray powder patterns indicate some crystallinity (Figure 2) as stated above. For longer reaction times (hours), the materials show no sign of crystallinity. The Cu materials prepared from method 3 provide highly crystalline solids according to X-ray powder patterns, but the relative crystallinity did not change with the change in reaction times and temperatures. Similarly, for all $\{[\text{Ag}(\text{dmb})_2]Y\}_n$ polymers, there was no success in increasing the amorphous fraction of the materials by these variations of parameters.

(34) The X-ray powder diffraction pattern of the solid $\{[\text{Ag}(\text{dmb})_2]\text{CH}_3\text{CO}_2\}_n$ polymer has also been investigated and compared to that of the NO_3^- analogue. Like the other polymeric materials, the spectra are characterized by a crystalline section leading to sharp signals and an amorphous part inducing a relatively high baseline. Based upon the comparison of the X-ray powder diffraction pattern, the $\{[\text{Ag}(\text{dmb})_2]\text{NO}_3\}_n$ polymer is not isostructural to the other materials although some similar peaks are observed. A typical pattern spectrum and peak position data are provided in the Supporting Information. During the indexing processes, four possible solutions were obtained. Three of them did not index important lines and were not favored. The last one provides the following lattice parameters: $a = 23.018$ Å, $b = 37.111$ Å, $c = 15.645$ Å, and $\alpha = \beta = \gamma = 90^\circ$ (volume = 13363.93 Å³). This is one possible solution; others may also exist.

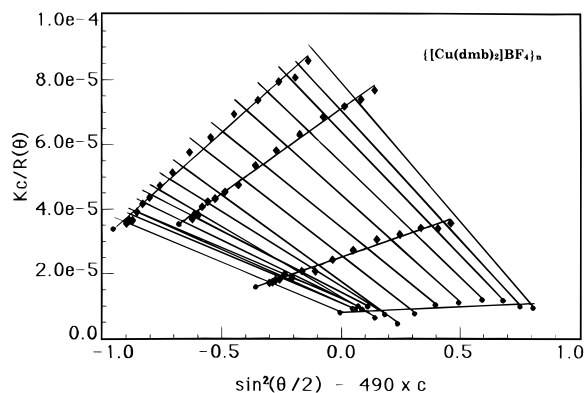


Figure 3. Typical Zimm plot associated with light diffusion measurements. Only three concentrations are shown for clarity: 0.07%, 0.14%, and 0.19%. Polymer: amorphous {[Cu(dmb)₂]BF₄}_n.

scattering techniques.³⁵ Figure 3 shows a typical Zimm plot from which the M_w values are extracted. From the numerous measurements all the Zimm data indicate that the M_w ranges from 1.27×10^5 to 1.92×10^5 as stated above, averaging $\sim 1.60 \times 10^5$. This technique does not provide information on the M_w distribution, although it appears that this may vary sensitively from one sample to another based upon the X-ray powder diffraction patterns. The dn/dc parameter (delta refraction index/delta concentration (in g/100 mL)) measured by differential refractometer is 0.13.

At such M_w values, the average chain number of “[Cu(dmb)₂]BF₄” units would vary between 240 and 360. A typical polymer containing 300 units would be 0.15 μm long when completely linear. Such a value would be theoretically comparable to a low molecular weight polyethylene sample of about 1000 units (28 000, $\sim 0.13 \mu\text{m}$) when stretched.

For the isostructural {[Ag(dmb)₂]BF₄]_n polymer for which solubility in acetonitrile is comparable to that of the Cu analogue, the results indicated that the M_w is $\leq 10\,000$ (i.e. ≤ 18 units), at least for the few samples that were analyzed. Due to their high crystallinity behavior, we conclude that these materials must be oligomeric in nature. The lower number of units in this case is consistent with the fact that crystals suitable for X-ray analysis were obtained, while no crystal was obtained for the Cu polymer. For the {[Ag(dmb)₂]PF₆]_n material, major solubility problems were encountered in various solvents and could not be investigated. The {[Ag(dmb)₂]NO₃]_n polymer constantly precipitated as a function of time producing deposits on the inner walls of the spectroscopy cells. No measurement could be taken.^{36,37} For the two other Cu polymers (Y = ClO₄⁻, NO₃⁻), data were obtained and indicated that the M_w are $\leq 10\,000$ also.

In these cases, electrospray technique and FAB mass spectrometry were also used. Unfortunately, the electrospray measurements failed. The FAB mass spectra exhibit several weak signals at weights ranging from 1000–2000 g. The largest signal is “Ag(dmb)₂Y” and exhibits the appropriate isotopic pattern.

(35) (a) Prud'homme R. E. *Synthèse et Caractérisation des Macromolécules, Manuel de Travaux Pratiques*; La Presse de l'Université Montréal: Montréal, 1981; ISBN 2-7606-0420-9. See also: (b) WYATT TECHNOLOGY CORPORATION; Manual Software DAWN Vesion 1.01; Wyatt Technology Corporation, 802 E. Cota Street P. O. Box 3003, Santa Barbara, CA 93130; 1993; pp 1–44. (6) WYATT TECHNOLOGY CORPORATION; Aurora Software Manual, Wyatt Technology Corporation, 802 E. Cota Street, P. O. Box 3003, Santa Barbara, CA 93130; 1993; pp 1.1–5.26.

(36) The polymers are reasonably soluble in DMSO. Unfortunately solvent parameters necessary for the evaluation of the Zimm plot are not known.

4. Calorimetric Properties. The polymeric materials are all microcrystalline at room temperature. Upon increasing the temperature, the polymers become wax-like molten glass at temperatures above 35 °C attributable to a glass transition. From DSC, the change in heat capacities (C_p) associated with the phase transition range from 0.1 to 1.3 (J/g)·deg indicating that the phase transition is second order. With further increases in temperature (> 130 °C) decomposition is observed as the white or pale beige materials turns black or brown irreversibly. TGA measurements confirmed the weight loss of the samples. In none of the polymers reported in this work was melting observed (using melting point apparatus). Table 2 presents the calorimetric data (T_g and T_d , decomposition temperatures) obtained

(37) (a) In an attempt to demonstrate that the highly crystalline materials are of low molecular weight, the spin–lattice relaxation times have been measured by ¹³C-NMR spectroscopy. At 75.47 MHz and for low molecular weight (< 1000), the systems are within the extreme narrowing limits. If one assumes that T_1 is solely dominated by dipolar interactions, then T_1 is given by:^{37b}

$$T_1^{-1} = \sum_{i=1}^n \gamma_C^2 \gamma_H^2 h^2 \tau_c / r_{CH_i}^6$$

where γ_C and γ_H are the magnetogyric ratios for ¹³C and ¹H nuclei, h is the Planck constant, r_{CH_i} is the ¹³C–¹H distance (2.15–2.16 Å according to molecular modelings; see scheme in the Supporting Information) and τ_c is the correlation time. For the mononuclear [M(CN-*t*-Bu)₄]BF₄ complexes (M = Cu, Ag), the spherical model relating τ_c and the molecular dimensions is used:

$$\tau_c = 4\pi a^3 \eta / 3kT$$

where a is the radii of the molecule, k is the Boltzmann constant, η is the viscosity of the medium (acetonitrile in this case), and T is the temperature. The ¹³C-NMR signal of the quaternary carbone is used for the measurements, and the experimental T_1 's are 12.5 ± 0.1 and 33.8 ± 0.1 s for M = Cu and Ag, respectively. In these cases the calculated “ a ” values are 6.5 and 4.7 Å, respectively. Molecular models predict that these radii are ~ 7.3 and 7.5 Å, respectively. This comparison is reasonable, although slightly under estimated. If one adds other contributions such as a quadrupolar relaxation process for instance, then the calculated τ_c 's decrease, and the obtained “ a ” values decrease as well, worsening the comparison. We conclude that T_1 must be dominated by dipole–dipole interactions in these compounds, and the polymers as well. For the crystalline polymers for which we expect molecular weights of $\sim 10\,000$, one cannot safely assume that these systems are within the extreme narrowing conditions. The general equation for T_1 is:^{37c}

$$T_1^{-1} = \sum_{i=1}^n \frac{\gamma_C^2 \gamma_H^2 h^2 \tau_c}{20r_{CH_i}^6} [2/(1 + (\omega_H - \omega_C)^2 \tau_c^2) + 6/(1 + \omega_C^2 \tau_c^2) + 12/(1 + (\omega_H + \omega_C)^2 \tau_c^2)]$$

where $\omega = \gamma H_0$ with H_0 being the external field (7.06×10^4 G). The ¹³C-NMR signals used for the measurements are the 63.2 and 62.8 ppm peaks for M = Cu and Ag, respectively, which correspond to carbon 8 in Figure 6. The graph of T_1 vs τ_c gives a minimum at $\tau_c \sim 1.05 \times 10^{-8}$ s and $T_1 \sim 6.2$ s (Supporting Information). For the {[M(dmb)₂]BF₄]_n polymer the experimental T_1 's are 6.1 ± 0.1 and 6.6 ± 0.1 s for M = Cu and Ag, respectively. The corresponding τ_c 's are $\sim 1.05 \times 10^{-8}$ s (one value only) for M = Cu and $\sim 7 \times 10^{-9}$ and 1.55×10^{-8} s for M = Ag. By replacing $4\pi a^3/3$ (volume of a sphere) by $\pi a^2 b$ where b is the length of a cylindrical molecule, the molecular dimension b can now be estimated:

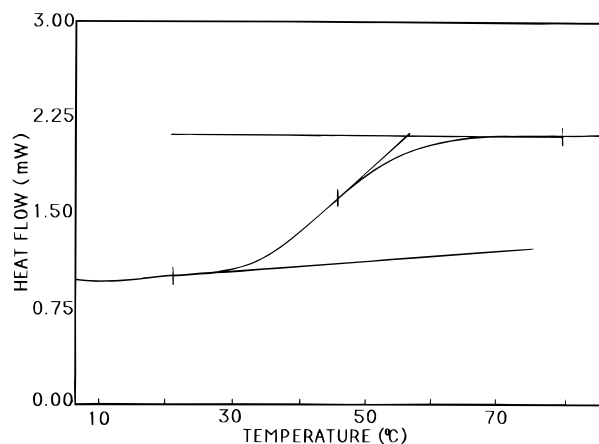
$$\tau_c = \pi a^2 b \eta / kT$$

where $a = 7.3$ and 7.5 Å for M = Cu and Ag, respectively. This equation predicts $b = 37$ Å for M = Cu (~ 8 Cu(dmb)₂ units) and $b = 24$ Å (if $\tau_c = 7 \times 10^{-9}$ s, i.e. ~ 5 Ag(dmb)₂ units) or 52 Å (if $\tau_c = 1.55 \times 10^{-8}$ s, i.e. ~ 12 Ag(dmb)₂ units). If the above 6.5 (M = Cu) and 4.7 Å (M = Ag) “ a ” values obtained for the mononuclear complexes are used, then the b values extracted are 47 Å (~ 10 Cu(dmb)₂ units), 60 Å (for $\tau_c = 7 \times 10^{-9}$ s, i.e. ~ 12 –13 Ag(dmb)₂ units), and 133 Å (for $\tau_c = 1.55 \times 10^{-8}$ s, i.e. ~ 28 Ag(dmb)₂ units). T_1 for {[Ag(dmb)₂]NO₃]_n is 7.1 ± 0.1 s and suggests that its M_w should be in the same order of magnitude to that of the BF₄⁻ samples. These measurements clearly indicate that these materials are oligomeric. (b) Levy, G. C.; Lichter, R. L.; Nelson, G. L. *Carbon-13 Nuclear Magnetic Resonance Spectroscopy* 2nd ed.; Wiley: Toronto, 1980; Chapter 8, p 211. (c) Wehrli, F. W.; Wirthlin, T. *Interpretation of Carbon-13 NMR Spectra*; Heyden: London, 1980, p 133.

Table 2. Glass Transition and Decomposition Temperatures

polymers	morphology	$T_g/\pm 5^\circ\text{C}$	$T_d/^\circ\text{C}^a$
$\{[\text{Ag}(\text{dmb})_2]\text{BF}_4\}_n$	highly crystalline	38–44	165–166
$\{[\text{Ag}(\text{dmb})_2]\text{PF}_6\}_n$	highly crystalline	<i>b</i>	170–171
$\{[\text{Ag}(\text{dmb})_2]\text{CH}_3\text{CO}_2\}_n$	highly crystalline	37	~180
$\{[\text{Ag}(\text{dmb})_2]\text{NO}_3\}_n$	highly crystalline	58	133–134
$\{[\text{Ag}(\text{dmb})_2]\text{ClO}_4\}_n$	highly crystalline	40	168–170
$\{[\text{Cu}(\text{dmb})_2]\text{BF}_4\}_n$	highly crystalline	<i>b</i>	176
	semicrystalline	57	178
	amorphous	45	165
$\{[\text{Cu}(\text{dmb})_2]\text{NO}_3\}_n$	amorphous	79	148–150
$\{[\text{Cu}(\text{dmb})_2]\text{ClO}_4\}_n$	semicrystalline	96	140

^a T_d = decomposition temperature. These reported temperatures have been obtained from both DSC and melting point apparatus. The decomposition process has been observed from the irreversible change of color going from white or beige to black or brown. The possibility that the materials undergo melting with simultaneous decomposition still exists. ^b No T_g has been observed between -100 to 170°C .

**Figure 4.** Typical DSC curve for solid $\{[\text{Cu}(\text{dmb})_2]\text{BF}_4\}_n$. Scan rate $10.0^\circ\text{C}/\text{min}$.

from DSC and TGA, respectively. The T_d data are the same using a melting point apparatus and a TGA instrument, and Figure 4 shows a typical DSC trace of a glass transition in these materials. The T_g values were found to be strongly scan rate dependent (T_g increases with the scan rate).

The intensity of the glass transition decreases with increased crystallinity, and crystallinity is dependent on thermal history. Finally the T_g behavior spreads over almost 50°C for some Ag polymers, notably for $Y = \text{NO}_3^-$. For the $\{[\text{Cu}(\text{dmb})_2]\text{BF}_4\}_n$ materials, the T_g spreads over only 20°C . The larger spread indicates that the materials exhibit highly dispersive crystalline domains (i.e. crystalline domains of very different sizes). By changing the synthesis conditions (reaction times, stoichiometry, and temperature), the T_g spread changes only a little.

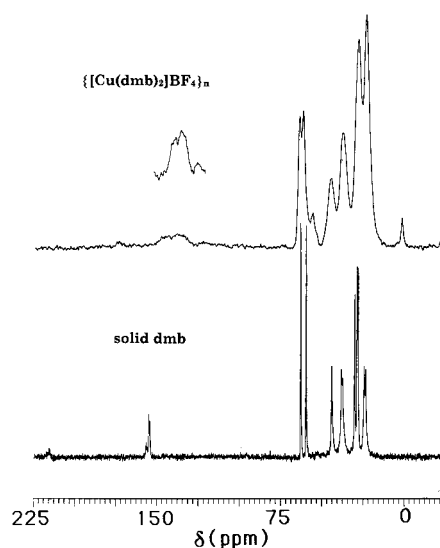
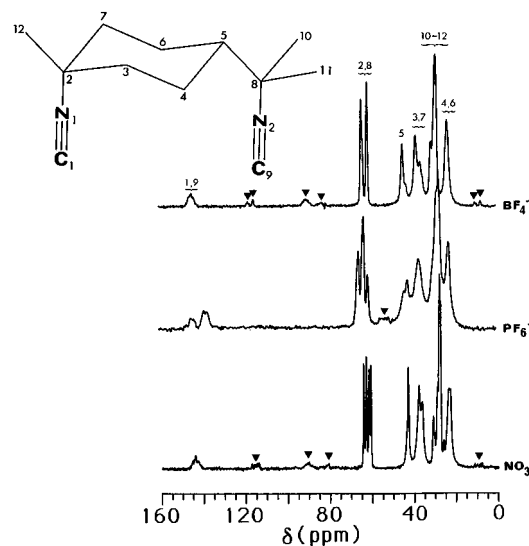
5. Solid-State ^{13}C -NMR Properties. The MAS (magic angle spinning) ^{13}C -NMR data for the free dmb ligand and the polymers in the solid state are now interpreted (Table 3).³⁸ The key feature of these data is that there are very little or no chemical shift differences between the compounds within 3ppm, except for the ^{13}C of the isocyanide group (within 15 ppm). The trend is as follows: δ free dmb $>$ $\delta\{[\text{Ag}(\text{dmb})_2]Y\}_n >$ $\delta\{[\text{Cu}(\text{dmb})_2]\text{BF}_4\}_n$, which is consistent with the presence of coordination chemistry (σ -donor and π -acceptor) at the isocyanide C atoms. One interesting observation is the great variation of the bandwidth between the materials (Figures 5 and 6). The bandwidth varies as free dmb $<$ $\{[\text{Ag}(\text{dmb})_2]Y\}_n <$ $\{[\text{Cu}(\text{dmb})_2]\text{BF}_4\}_n$, and is essentially crystallinity dependent where highly amorphous materials give broader MAS ^{13}C -NMR

(38) The ^{13}C -NMR spectra of the polymers in CD_3CN solution at 298 K were also analyzed and are provided in the Supporting Information.

Table 3. MAS ^{13}C -NMR δ Values for Selected Polymers and Free dmb in the Solid State at $298\text{K}^{a,b}$

C no.	free ligand	$\{[\text{Ag}(\text{dmb})_2]\text{NO}_3\}_n$	$\{[\text{Ag}(\text{dmb})_2]\text{BF}_4\}_n$	$\{[\text{Ag}(\text{dmb})_2]\text{PF}_6\}_n$	$\{[\text{Cu}(\text{dmb})_2]\text{BF}_4\}_n$
1	155.5	144 m	145 m	145	140 br
9	155.9			139	
2	62.5	64, 63	64	66, 63	64 br
8	59.1	62, 63	61	61	62 br
5	43.6	43	45, 42	42	45 br
6	24.0	24 br	23	23	23 br
4	23.1				
7	37.7	38	38	37	38 br
3	37.0	36	36		
12	29.7	31, 29	31	27	28 br
10	28.1	26, 28	29	27	28 br
11	27.6				

^a m = multiplet. br = broad. ^b The C no. refers to that posted in Figure 6. Data for $\{[\text{Cu}(\text{dmb})_2]\text{BF}_4\}_n$ are from the amorphous samples.

**Figure 5.** Comparison of the MAS solid-state ^{13}C -NMR spectra of the amorphous $\{[\text{Cu}(\text{dmb})_2]\text{BF}_4\}_n$ polymer and free dmb. The peak assignments are all provided in Table 3.**Figure 6.** Comparison of the MAS solid-state ^{13}C -NMR spectra of the $\{[\text{Ag}(\text{dmb})_2]Y\}_n$ polymers: $Y = \text{BF}_4^-, \text{PF}_6^-, \text{NO}_3^-$. The peak assignments are provided in Table 3.

signals. The crystallinity is qualitatively deduced from the X-ray powder diffraction patterns described earlier.

The MAS ^{13}C -NMR signals for carbons 1, 2, 9 and 8 (numbering referring to Figure 6) in the $\{[\text{Ag}(\text{dmb})_2]Y\}_n$ spectra

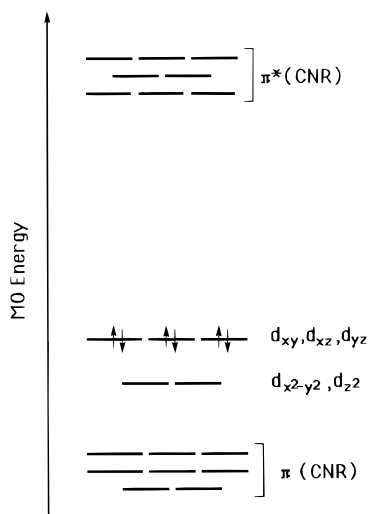


Figure 7. Qualitative energy MO diagram for a tetrahedral monomeric ML_4^+ species ($L = CNR$ where R is H).

($Y = BF_4^-, PF_6^-, NO_3^-$) are either very broad (carbons 1 and 9) or split into many components (carbons 12 and 8). The phenomenon is clearly associated with different chemical environments of the C atoms. A deconvolution of the “triplet” associated with the ^{13}C -NMR signal of carbons 2 and 8 in $\{[Ag(dmb)_2]PF_6\}_n$ reveals that this series of bands is in fact two doublets. Two possible explanations for this result are the following: (1) the $Ag-C$ and $N-C$ bond distances are different in some cases around the distorted tetrahedral Ag metal, and (2) the head-to-tail and head-to-head $dmb-dmb$ interactions are present along the chains. The analysis of the ^{13}C -NMR spectra (in carbons 2 and 8) is not a simple one, and cannot be dealt with due to the uncertainties on the bond lengths, the presence of disorder in the dmb ligand, and the bandwidth of the ^{13}C -NMR signals.

In an attempt to characterize the glass transitions of the polymers, the temperature dependence of the MAS- ^{13}C -NMR spectra is investigated. From room temperature up to 398 K, the spectra were identical showing very little or no chemical shift change, and no change in bandwidth, for each sample investigated. This result indicates that the chemical environment of the C atoms does not change greatly through the glass transition. One can safely speculate that the polymers in the high-temperature phase do not greatly deviate from their tubular structure, and therefore the gain in material mobility (or decrease in viscosity) must be attributed to an increase in ionic mobility of the counteranions. The experimental support for this hypothesis is found in the decrease in electrical resistivity in the glass phase. These materials are all insulating at 298 K, but their electrical conductivities reach the semiconducting/conducting limit above the phase transition. This change in electric conductivities occurs rapidly at the phase transition.

6. Optical Properties and MO Calculations. The nature of the lowest energy excited states has been addressed using the density functional theory on the monomeric model compound $M(CNH)_4^+$ (Chart 4) prior to investigating the luminescence properties. These model compounds are chosen to reduce the size of the computations (H atoms vs alkyl groups). The MO diagram is shown in Figure 7 and a description of the atomic orbital electronic density contributions to the MO's is provided in Table 4. The LUMO and the HOMO are $7t_2$ and $6t_2$, respectively. The $7t_2$ MO is composed mostly of C and N p_x and p_y π orbitals, but the C-N interactions are antibonding. The HOMO is largely composed of metal d_{xy} , d_{yz} , d_{xz} contributions (51%) and C s components (24%). The HOMO-1 (located

Table 4. Atomic Orbital Contributions^a

MO	energy (eV)		contributions ^b							
	Ag	Cu	Ag		C		N		H	
			d_{xy}, d_{yz}	$d_{z^2}, d_{x^2-y^2}$	s	p	s	p	s	p
$6a_1$	-2.751	-2.652			100					
$8t_2$	-3.174	-3.216							10	88
$5a_1$	-3.385	-3.454							10	77
$2t_1$	-4.664	-4.583					68	31		
$3e$	-4.942	-5.139					64	28		
$7t_2$ (LUMO)	-5.299	-5.486					58	26		
$6t_2$ (HOMO)	-10.695	-10.207	51			9	24			
$2e$	-12.299	-11.052		86				12		
$1t_1$	-13.689	-13.735				32		66		
$5t_2$	-13.774	-13.834				35		62		
$1e$	-13.912	-14.026			12	32		55		

^a Contributions of less than 5% are not tabulated. ^b Only the contributions for Ag are tabulated. The relative ratio for the atomic contributions in $Cu(CNH)_4^+$ is practically the same as that for the $Ag(CNH)_4^+$ compound.

Table 5. Calculated Lowest Energy Singlet-Singlet Electronic Transitions for the $M(CNH)_4^+$ Model Compounds ($M = Cu, Ag$)

transition	label	calculated energy/nm	
		$Cu(CNH)_4^+$	$Ag(CNH)_4^+$
$6t_2 \rightarrow 7t_2$	$d \rightarrow \pi^*$ (CNH) i.e. MLCT	263	230
$6t_2 \rightarrow 3e$	$d \rightarrow \pi^*$ (CNH) i.e. MLCT	245	215
$6t_2 \rightarrow 2t_1$	$d \rightarrow \pi^*$ (CNH) i.e. MLCT	220	206
$2e \rightarrow 7t_2$	$d \rightarrow \pi^*$ (CNH) i.e. MLCT	223	177
$2e \rightarrow 3e$	$d \rightarrow \pi^*$ (CNH) i.e. MLCT	210	169

~ 1.6 eV below; i.e. 12900 cm^{-1}) is composed of the M d_{z^2} , $d_{x^2-y^2}$ orbitals (86%) in agreement with the ligand field theory. Below the filled M d orbitals lie near three other closely located MO's. These are $\pi(CNH)$ MO's with little or no metal contributions. Above the LUMO lie the $3e$, $2t_1$, $5a_1$, $8t_2$, and $6a_1$ MO's. The $3e$ and $2t_1$ are other $\pi^*(CNH)$ orbital energy levels. These are located closely to the LUMO (0.357 and 0.635 eV, respectively) and exhibit similar atomic contributions to that of the LUMO. Above these eight $\pi^*(CNH)$ MO's lie two sets of MO's, $5a_1$ and $8t_2$, which are the high energy $\sigma^*(N-H)$ bond antibonding orbitals. These are of little consequence to this work and are not dealt with in this study. Finally, the $6a_1$ (located ~ 8 eV above the HOMO) is the M s orbital. Based upon these calculations, the lowest energy electronic transition is predicted to be $6t_2$ (d_{xy} , d_{yz} , d_{xz}) $\rightarrow \pi^*(CNH)$, which is a metal-to-ligand charge transfer (MLCT). These results are in agreement with the EHMO and experimental findings for the $Ag_2(dmb)_2X_2$ complexes ($X = Cl, Br, I$),^{9a} and are different from that of the mono- and dimeric d^{10} Pd- and Pt-phosphine complexes ($d \rightarrow p$).³⁹ Based upon the calculated energy gap between the LUMO and the HOMO (Table 4), the lowest energy electronic bands should be located in the ~ 230 - and ~ 263 -nm range for $M = Ag$ and Cu , respectively. Experimentally, these values are very close to those observed for the monomeric species $M(CN-t-Bu)_4^+$ (± 30 nm; Table 5, Figure 8). In general, good agreements between the calculated and experimental data for inorganic compounds have been observed before with the density functional theoretical computations.⁴⁰ The absorptivity data at λ_{max} are as follows: $[Ag(CN-t-Bu)_4]BF_4$, 6700; $[Cu(CN-t-Bu)_4]BF_4$, 9500; $\{[Ag(dmb)_2]Y\}_n$; $Y = PF_6^-$, 9500; $Y = BF_4^-$, 6700; $Y = CH_3CO_2^-$, 8900; $Y = NO_3^-$, 17500; $\{[Cu(dmb)_2]BF_4\}_n$, 7000 $M^{-1}\text{ cm}^{-1}$.

(39) (a) Harvey, P. D.; Schaefer, W. P.; Gray, H. B. *Inorg. Chem.* **1988**, 27, 1101. (b) Harvey, P. D.; Gray, H. B. *J. Am. Chem. Soc.* **1988**, 110, 2145.

(40) See for example: Harvey, P. D.; Hubig, S.; Ziegler, T. *Inorg. Chem.* **1994**, 33, 3700.

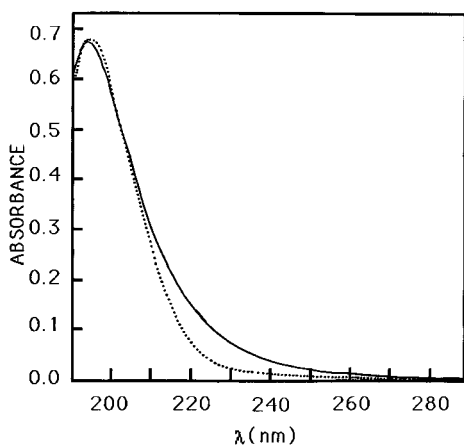


Figure 8. Comparison of the UV spectra of the $[\text{Ag}(\text{CN-}t\text{-Bu})_4]^+$ (dotted line) and $\{[\text{Ag}(\text{dmb})_2]Y\}_n$ (straight line) materials ($Y = \text{BF}_4^-$) in acetonitrile at 298 K. The ϵ values are 8000 and 6700 $\text{M}^{-1} \text{cm}^{-1}$ for the monomer and polymer, respectively ($M = \text{Ag}$ at ~ 200 nm).

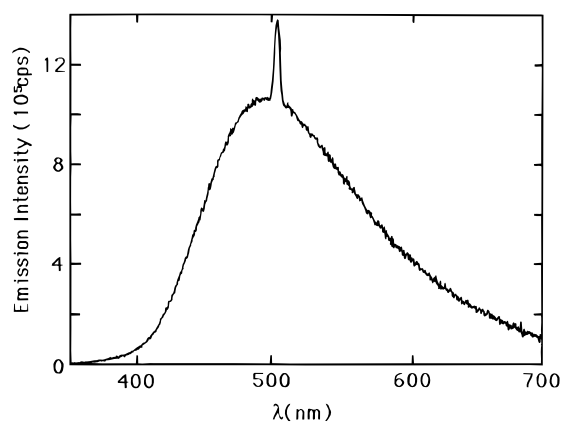


Figure 9. Typical emission spectrum of the polymer $\{[\text{Ag}(\text{dmb})_2]\text{PF}_6\}_n$ in KBr pellets at 77 K. The excitation wavelength is 250 nm. The sharp peak at 500 nm is the first harmonic of the 250-nm excitation (instrumental artifact).

Table 6. Emission λ_{max}^a

compd	λ_{max} (nm)		
	EtOH at 77 K	solid state at 77 K	KBr pellets at 77 K
$[\text{Cu}(\text{CN-}t\text{-Bu})_4]\text{BF}_4$	510	490	514
$\{[\text{Cu}(\text{dmb})_2]\text{BF}_4\}_n$	548	517	550
$[\text{Ag}(\text{CN-}t\text{-Bu})_4]\text{BF}_4$	435	474	467
$\{[\text{Ag}(\text{dmb})_2]\text{BF}_4\}_n$	502	486	510
$\{[\text{Ag}(\text{dmb})_2]\text{PF}_6\}_n$	484	467	467
$\{[\text{Ag}(\text{dmb})_2]\text{NO}_3\}_n$	435	489	499
$\{[\text{Ag}(\text{dmb})_2]\text{CH}_3\text{COO}\}_n$	454	492	492

^a The uncertainties on λ_{max} are ± 5 nm.

7. Emission Properties. These materials are found to be weakly luminescent at room temperature, but exhibit intense blue emissions at lower temperatures (i.e. 77 K). The emission bands are generally located at around 500 nm (Figure 9 and Table 6), and all appear to be vibrationally unstructured. The emission maxima (λ_{max}) are found to be both medium and counteranion dependent. The monomeric species ($M(\text{CN-}t\text{-Bu})_4^+$; $M = \text{Cu}, \text{Ag}$) have been specifically selected in order to study the presence of the very long $M \cdots M$ interactions (Scheme 1) if any. The difference in λ_{max} between the monomeric and polymeric species ($Y = \text{BF}_4^-$) suggests that $M \cdots M$ interactions may indeed play a role in the stabilization energy of the emissive state.

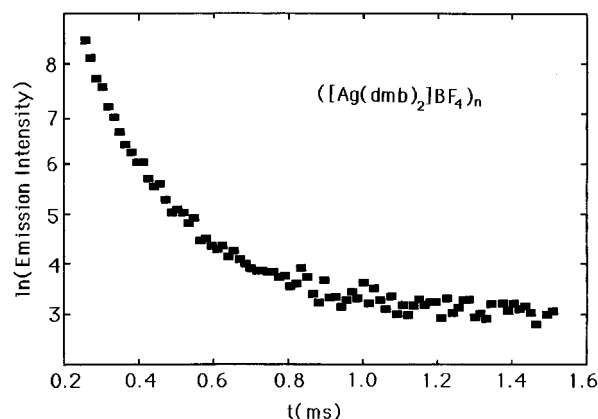
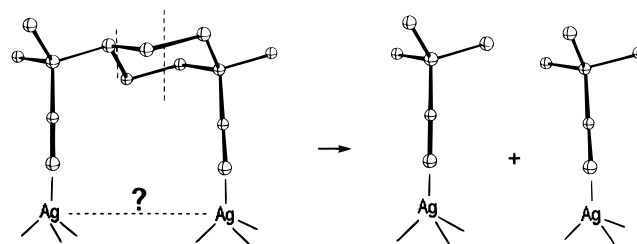


Figure 10. Typical example of an emission decay trace (ln scale) for the polymeric material showing the polyexponential behavior. In this example $\{[\text{Ag}(\text{dmb})_2]\text{BF}_4\}_n$ in KBr pellets at 77 K is used. No single lifetime describing the full deactivation trace can be obtained from these measurements. Details of the analysis is given in Table 7.

Scheme 1



The emission decays for both monomeric samples (in ethanol solutions, solid state fine powders or single crystals at 77 K) exhibit typical monoexponential kinetics (see Supporting Information for a typical example). On the other hand, the emission decay traces for the polymers are polyexponential⁴¹ (in ethanol, fine powder, and single crystal; see Figure 10 for an example). The emission lifetimes range from 7 to ~ 600 μs , and are typical of emissions arising from a triplet MLCT state with a metal in its d^{10} electronic configuration.⁴² The comparison of the decay traces of the same polymer ($M = \text{Cu}$, $Y = \text{BF}_4^-$; $M = \text{Ag}$, $Y = \text{BF}_4^-, \text{PF}_6^-, \text{NO}_3^-, \text{CH}_3\text{CO}_2^-$) in ethanol or in powder or crystalline form at 77 K show some differences (Table 7). Three important tendencies are observed. (1) The powder and large single crystals data are very similar. For instance the τ_e and I_{rel} values for $\{[\text{Ag}(\text{dmb})_2]\text{CH}_3\text{CO}_2\}_n$ are $\tau_1 = 11.65$ μs , $I_1 = 76.0\%$, $\tau_2 = 36.3$ μs , $I_2 = 22.9\%$, $\tau_3 = 166.8$ μs , and $I_3 = 1.1\%$ (see powder data in Table 7 for comparison). (2) The powder data have the tendency to require more exponential components than the ethanol data. This information indicates that the deactivation processes in the solid state exhibit other deactivation pathways not available in solution. These supplementary processes clearly originate from interchain energy transfers, similar to the solid state exciton phenomenon. (3) The first component lifetimes for the powder data are always shorter than that of ethanol. The last observation is a simple consequence of the presence of the supplementary processes in the decay traces. By comparing the powder data, the first component τ_e values vary as $\text{BF}_4^- > \text{PF}_6^- > \text{NO}_3^- > \text{CH}_3\text{CO}_2^-$, and indicate that the counteranions play a role in the overall deactivation mechanism.

(41) The criteria used to decide the number of components necessary to describe the data is based on the first best fit where all the data points are reasonably well fitted, going from a mono-, to bi-, and to tri-, and to tetraexponential analysis. These results indicate that the polymeric nature of the materials clearly influences the excited state deactivation pathways.

(42) See for example Harvey, P. D.; Gray, H. B. *Polyhedron* **1990**, *9*, 1949 and the references therein.

Table 7. Emission Lifetime Analysis^a

compd	powder at 77 K		EtOH at 77 K	
	rel intensity	$\tau_e/\mu\text{s}$	rel intensity	$\tau_e/\mu\text{s}$
[Cu(CN- <i>t</i> -Bu) ₄]BF ₄	100	36.6	100	36.8
[Ag(CN- <i>t</i> -Bu) ₄]BF ₄	100	59.3	100	47.6
{[Cu(dmb) ₂]BF ₄ } _n	34.6	38.8	67.3	45.9
	56.9	72.3	31.2	101.1
	7.1	183.0	1.4	352.4
	1.4	289.3		
	68.0	44.6	39.5	(10.9)
{[Ag(dmb) ₂]BF ₄ } _n ^b	26.6	137.5	60.4	70.5
	4.5	564.4		
	0.9	4.77 × 10 ⁶		
	57.2	19.3	90.2	26.5
{[Ag(dmb) ₂]PF ₆ } _n	39.2	53.5	9.8	151.6
	3.4	242.8		
	0.3	490.4		
	62.3	14.8	83.9	31.6
{[Ag(dmb) ₂]NO ₃ } _n	32.4	38.7	14.0	96.5
	4.9	146.1	2.1	126.0
	0.44	584.5		
	89.0	(7.1)	82.5	30.2
{[Ag(dmb) ₂]CH ₃ COO} _n	10.3	35.5	17.5	151.6
	1.0	194.9		

^a Single crystal data and powder data were very similar. The details for the few single crystal data analysis are not included. The data analyses were performed by a deconvolution technique. The data in parentheses are considered not to be accurate; they are close in size to the time domain of the lamp pulse. ^b The tetraexponential fit is best in this case but reasonable fits are obtained for a triexponential analysis: $I_1 = 76.6\%$, $\tau_1 = 49.6 \mu\text{s}$, $I_2 = 21.3\%$, $\tau_2 = 200.8 \mu\text{s}$, $I_3 = 2.1\%$, $\tau_3 = 3060 \mu\text{s}$. The biexponential fit is not as good: $I_1 = 78.4\%$, $\tau_1 = 49.2 \mu\text{s}$, $I_2 = 21.4\%$, $\tau_2 = 118.5 \mu\text{s}$. In this case the data points showed some scatterings.

The polyexponential behavior of the emission decays of the polymer dissolved in ethanol is now addressed. The short-lived component (which represents ~70% of the total intensity) exhibits a lifetime of ~46 μs in {[Cu(dmb)₂]BF₄}_n. This datum is within the same order of τ_e magnitude of the datum for [Cu(CN-*t*-Bu)₄]BF₄ (~37 μs). Similarly, the same observation is made for the Ag materials averaging ~25 μs ($\tau_e = 48 \mu\text{s}$ for [Ag(CN-*t*-Bu)₄]BF₄). This comparison worsens with the second and third components (Table 7). The time-resolved emission spectra for the polymers in ethanol and in the solid state have been obtained at 77 K. For the short-lived species (i.e. at time windows located at the beginning of the decay traces), the measured emission spectra are blue-shifted (relative to the non-time-resolved data) exhibiting λ_{max} approaching the λ_{max} obtained for the mononuclear compounds. At longer delay times after the light pulses, the measured emission spectra are sensitively red-shifted (up to ~50 nm; for a typical example see Figure 11). Such a result explains the large width and the long tail of the emission bands (see Figure 9 as an example). There is no evidence of the presence of an isosbestic point in the series of time-resolved emission spectra for the powder and ethanol data. The time-resolved progression of the spectra appears to be continuous where a regular red-shift of the emission band is observed as a function of delay time after the pulses. The reasonable comparison in τ_e of the first component in the decay traces and in λ_{max} in the early emission spectra of the polymeric materials and the M(CN-*t*-Bu)₄⁺ complexes indicates that the excited state deactivations of the short-lived species in the polymers are associated with "isolated" ML₄^{*} fragments behaving like mononuclear complexes with no M...M interactions. Generally, this deactivation process is dominant (Table 7). The remainder of the emissions which are red-shifted and longer lived are associated with delocalized (ML₄)_n^{*} units involving an energy transfer within the backbone.^{43,44}

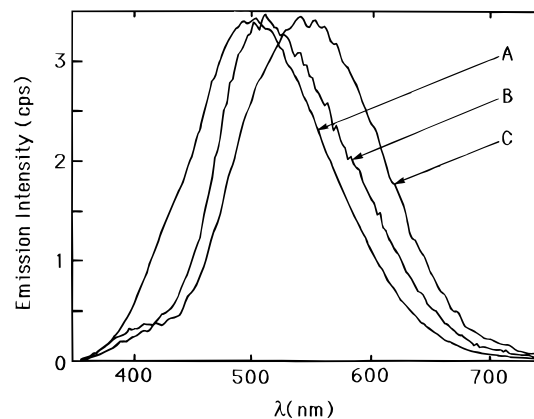


Figure 11. Time-resolved spectra for solid {[Ag(dmb)₂]BF₄}_n at 77 K: spectrum A, between 40 and 280 μs ; spectrum B, between 280 and 520 μs ; spectrum C, between 520 and 760 μs .

There have been a number of literature cases where energy transfer processes were demonstrated to occur within polymers.^{7c,11,45} Generally three methods are employed to investigate these phenomenon. The first one is the emission quenching experiments using polymers and monomers. Second is the emission investigations of the copolymers. Third is the measurements of the polarization ratios of the emission light. The first two methods are not applicable in this case, since both the polymers and the complexes absorb in the same spectral region (Figure 8), and since the preparation of copolymers in these cases is unknown. Therefore, the third method is employed. The polarization ratios (N) were measured using 235-nm excitation in ethanol as a solvent at 77 K. Perfectly polarized emissions give $N = 3.0$ or 0.5 . Depolarized light gives $N = 1$. Experimentally we obtained this later value all along the emission spectra (Supporting Information). This result corroborates the evidence for an energy-transfer process.

(43) The presence of these long-lived and red-shifted species is obviously not generated by electron transfer, nor by the presence of ground-state metal-metal interactions (as the UV-visible spectra of the mononuclear and polymer species are very similar). The presence of excimer type emission is also a difficult interpretation to adopt because for a fixed distance (~5 Å), the λ_{max} emission should also be constant with time delays (i.e. time-resolved measurements should exhibit two distinct emissions). One can also exclude the possibility of different polymer conformations in the solids and glasses since the materials are rigid rods. The presence of impurities is ruled out since the preparation of all materials (including the mononuclear species) has been performed with the same materials (except dmb was used instead of CN-*t*-Bu). The decay traces in the mononuclear species are rigorously monoexponential. Further dmb complexes (such as Ag₂(dmb)₂X₂; X = halogen) have been prepared and exhibit single exponential decay traces as well.^{9a} Finally the hypothesis of the presence of traps is considered but is also ruled out. "Traps" are solid-state properties, and solution data (where no trap exist) also exhibit polyexponential behaviors. The last possible interpretation is the metal-to-metal energy transfer along the chain, where the number of M atoms involved varies. This explanation is consistent with the presence of some interchain energy transfers deduced from the τ_e data (Table 4). There have been cases in the literature with organic polymers where polyexponential decays and multi-emissions are observed.⁴⁵ In these cases two very distinct emission bands were observed, one of which was related to the end-of-chain species, and the other one to middle chain. This is not the case here.

(44) The emission decay traces for the polymers in KBr pellets exhibit in all cases a significant increase in deactivation kinetic. The faster deactivation process is typical for external heavy atom effects. The polyexponential behavior of the kinetic traces is still present under these conditions but is less extensive. These results indicate that the lumophore (M(CNR)₄⁺), which appears to be isolated within the backbone of the polymers, is still able to sense external perturbation.

(45) (a) Guillet, J. *Polymer Photophysics and Photochemistry: An Introduction to the Study of Photoprocesses in Macromolecules*; Cambridge University Press: Cambridge, 1985. (b) Phillips, D.; Roberts, A. J., Eds. *Photophysics of Synthetic Polymers*; Science Review Ltd.: Northwood, 1982.

Final Remarks

These remarks concern the conductivity properties of these materials. Based upon their colors (white for Ag or beige for Cu), the measured high resistivity was easily predictable. We have attempted to make a mixed-valent polymeric material using a mixture of Cu(I) and Cu(II) starting material. We have indeed observed the typical deep purple color ($\lambda_{\text{max}} = 700$ nm) attributable to mixed-valence Cu(I)···Cu(II) centers,⁴⁶ but the reaction proceeded further where the color of the solution continued to change (deep purple \rightarrow deep orange \rightarrow pale yellow \rightarrow colorless). The final product was the polymeric $\{[\text{Cu}(\text{dmb})_2]\text{BF}_4\}_n$ material (i.e. Cu(I)). Reactions between $\text{Cu}^{\text{II}}(\text{BF}_4)_2$ and dmb also lead to the same product. Such redox reactions appear to utilize the dmb itself as a sacrificial reducing agent. No attempt was made to identify the organic product. We are aware of one other example of such chemistry with dmb where an Au(III) complex is reduced to an Au(I) compound.⁴⁷ In another attempt to prepare conductive materials, addition of I_2 was made with the hope that the overall reaction would be $\text{Cu}(\text{I}) + \frac{1}{2}\text{I}_2 \rightarrow \text{Cu}(\text{II}) + \text{I}^-$ (subsequently $\text{I}^- + \text{I}_2 \rightarrow \text{I}_3^-$). At that time we did not realize that Cu(II) and dmb also undergo redox reactions whether dmb was free or complexed. The sole inorganic product observed was $\text{Cu}_2(\text{dmb})_2\text{I}_2$ identified from X-ray analysis.⁴⁸ This complex is isostructural to the known $\text{Ag}_2(\text{dmb})_2\text{I}_2$.^{9d} From this work, it appears unlikely that conductivity could be achieved using the metal center as the

(46) Barr, M. E.; Smith, P. H.; Antholine, W. E.; Spencer, B. J. *Chem. Soc., Chem. Commun.* **1993**, 1649.

(47) Che, C.-M.; Wong, W.-T.; Lai, T.-F.; Kwong, H.-L. *J. Chem. Soc., Chem. Commun.* **1989**, 243.

(48) Reaction between $\{[\text{Cu}(\text{dmb})_2]\text{BF}_4\}_n$ and I_2 leads to the formation of $\text{Cu}_2(\text{dmb})_2\text{I}_2$ as identified from X-ray crystallography (as a di-ethanol solvate): space group $P2_1/n$, monoclinic, $a = 9.2630(12)$ Å, $b = 15.0150(20)$ Å, $c = 12.0438(16)$ Å, $V = 1650.3(4)$ Å³, $Z = 2$, $D_{\text{calc}} = 1.662$ g/cm³, $R = 0.137$, $wR = 0.164$. Selected bond distances and angles: $r(\text{Cu}\cdots\text{Cu}) = 3.199(10)$ Å, $r(\text{Cu}-\text{I}) = 2.726(7)$ and $2.785(6)$ Å; $r(\text{Cu}-\text{I}) = 1.90(4)$ and $1.80(4)$ Å; $\angle\text{I}-\text{Cu}-\text{I} = 109.03(19)^\circ$; $\angle\text{Cu}-\text{I}-\text{Cu} = 70.97(17)^\circ$; $\angle\text{C}-\text{Cu}-\text{C} = 144.5(17)^\circ$. The data are available in the Supporting Information.

“electron carrier”. We are now considering using ionic materials capable of electron conductivity and using the cationic polymeric chains solely to balance the charge and for their thermoplastic properties (if these could remain unchanged upon anion exchange). Preliminary results using the 7,7,8,8-tetracyanoquinodimethane anion (TCNQ^-) showed that conductivity in these polymers is possible, and will be reported in due course.

Acknowledgment. This research was funded by NSERC (Natural Sciences and Engineering Research Council) and FCAR (Fonds concertés pour l’avancement de la recherche). P.D.H. thanks Professor Robert Prud’homme (Université Laval, Québec) for allowing us to measure the molecular weights in his laboratory. P.D.H. is also thankful to Professors R. Brown (McGill University) and M. Leclerc (Université de Montréal) for fruitful discussion regarding the phase transitions and to Mr. Réjean Provencher (Sherbrooke) for his help with the theoretical calculations.

Supporting Information Available: Tables giving crystal data and details of the structure determination, all atomic coordinates, bond distances, bond angles, anisotropic thermal parameters, and torsion angles for $\{[\text{Ag}(\text{dmb})_2]\text{BF}_4\}_n$, $\{[\text{Ag}(\text{dmb})_2]\text{ClO}_4\}_n$, $\{[\text{Ag}(\text{dmb})_2]\text{NO}_3\}_n$, and $\text{Cu}_2(\text{dmb})_2\text{I}_2$ graph showing T_1 vs τ_c , scheme showing the nearest H neighbors to the quaternary C in the ligand, a stereoview of the $\{[\text{Ag}(\text{dmb})_2]\text{BF}_4\}_n$ polymer along with a view along the AgAgAg zigzag, tables and figures for the X-ray powder data for the $\{[M(\text{dmb})_2]Y\}_n$ polymers ($M = \text{Cu}, \text{Ag}; Y = \text{BF}_4^-, \text{ClO}_4^-, \text{CH}_3\text{CO}_2^-$), a table for ¹³C-NMR solution data, a comparison of the UV-vis spectra for $[\text{Cu}(\text{CN}-t\text{-Bu})_4]\text{BF}_4$ and $\{[\text{Cu}(\text{dmb})_2]\text{BF}_4\}_n$, a typical graph of $\ln I_e$ vs τ for $[\text{Ag}(\text{CN}-t\text{-Bu})_4]\text{BF}_4$, a figure showing the time-resolved spectra for solid $\{[\text{Cu}(\text{dmb})_2]\text{BF}_4\}_n$, and a graph of the polarization ratio vs λ_{em} for $\{[\text{Cu}(\text{dmb})_2]\text{BF}_4\}_n$ (44 pages). See any current masthead page for ordering and Internet access instructions.

JA9600845